Heliyon 10 (2024) e25612

Contents lists available at ScienceDirect

Heliyon

journal homepage: www.cell.com/heliyon

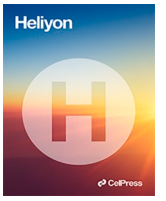

Research article

Assessment of asbestos-cement roof distribution and prioritized intervention approaches through hyperspectral imaging

David Enrique Valdelamar Martínez, Manuel Saba *, Leydy Karina Torres Gil

Civil Engineering Program, Universidad de Cartagena, Calle 30 # 48-152, Cartagena, Colombia

ARTICLE INFO

Keywords:
Asbestos roof identification
Asbestos in developing countries
AC weathering status
Strategies for AC removal in urban areas

ABSTRACT

The discernment of asbestos-cement (AC) roofs within urban areas stands as a pivotal concern pertinent to communal well-being and ecological oversight, particularly in emerging nations where asbestos continues to be extensively employed. Conventional methodologies entailing the recognition of asbestos-cement roofs and the characterization of their degradation status, such as tangible examinations and laboratory assays, prove to be temporally protracted, financially demanding, and arduous to extrapolate comprehensively across expansive urban domains. In this paper, it is presented a novel approach for identifying asbestos-cement roofs in urban areas using hyperspectral airborne acquisition and carry out a diagnosis that allows to identify the state of asbestos-cement roofs and thus provide a tool for the competent authorities to develop and prioritize intervention strategies to mitigate the problem. Four different methodologies were implemented and compared, three of which are new in the literature, to identify the deterioration of asbestos-cement (AC) roof state in large urban areas. This, in turn, furnishes a tool for competent authorities to identify the state of AC roofs, develop and prioritize intervention strategies to mitigate the problem.

The control points in field allowed validating the classification and the proposed methodology for the prioritization of intervention in AC roofs. Some neighborhoods in the city showed peaks in the area of asbestos-cement roofs of 47% of the total area of the neighborhood, representing practically all of the roofs present in the neighborhood. On average around 20% of the total area of a neighborhood in Cartagena is covered by AC. Furthermore, it was found a total area of AC roofs throughout the city of more than 9 km^2 (9 million square meters). On the other hand, two of the 4 methods used showed encouraging results that demonstrate their ability to identify covers in poor and good condition at a large scale from hyperspectral images. This academic novelty suggests that there is a possibility of practical application of these methods in other urban contexts with high concentrations of AC roofs, helping in the planning and optimization of intervention strategies to mitigate the risk in public and environmental health due to the presence of asbestos.

1. Introduction

Asbestos is a naturally occurring mineral widely used in construction materials due to its heat resistance, low conductivity, durability, and low cost. Many buildings around the world have asbestos such as homes, schools, hospitals, especially in roofs, walls

* Corresponding author.
E-mail address: msaba@unicartagena.edu.co (M. Saba).

https://doi.org/10.1016/j.heliyon.2024.e25612
Received 27 September 2023; Received in revised form 21 January 2024; Accepted 30 January 2024
Available online 6 February 2024

and floors. However, in the early 1900s it was discovered that asbestos exposure especially in air can lead to various health problems, including lung cancer, mesothelioma, and asbestosis among many others, [1–3].

Remote sensing technologies have revolutionized the field of environmental monitoring, providing a powerful tool for identifying and analysing materials spatial distribution, particularly in agriculture and geological exploration [4–6].

One of the areas where remote sensing have shown significant potential is in identifying asbestos-cement roofs, [6–8]. The development of control strategies and mitigation of asbestos related problems involves the identification of the material and its level of deterioration. Spectral sensor can be deployed on unmanned aircraft, manned aircraft, or satellites, with the choice influenced by the trade-off between spatial resolution (SRE) and economic factors. Unmanned aircraft provide high SRE but face logistical challenges for large-scale imaging. Manned aircraft offer a balanced SRE-to-cost ratio but are more common in developed countries. Satellite imagery, once considered less effective, has improved with technological advances, offering competitive SRE in both short-wave infrared (SWIR) and visible/near-infrared (VNIR) bands. This makes satellites attractive due to cost-effectiveness and ease of procurement without requiring flight permits [6].

Asbestos-cement (AC) identification methodologies center around computational algorithms such as object classification or object-based image analysis (OBIA) [9], Spectral Feature Fitting (SFF) [10], Spectral Angle Mapper (SAM) [7], Support Vector Machine (SVM) [11], decision trees and Random Forest (RF), discriminant function analysis (DFA) [12], and the maximum likelihood method (MLC), among other approaches. The employment of Convolutional Neural Networks (CNNs) has also been applied [13] for the discrimination of asbestos-cement tiles leveraging aerial RGB and color-infrared (CIR) imagery. Several studies can be found in literature regarding asbestos-cement roof classification through hyperspectral imagery, [13–15]. They normally display acceptable results with traditional [7], and innovative tools [13,16]. Bonifazi et al. (2022) [17] implemented a Classification and Regression Trees (CART) model to identify roofing materials containing asbestos amidst other objects through hyperspectral images acquired by the PRISMA satellite. The employed methodology demonstrated a noteworthy discriminatory capacity, as evidenced by high sensitivity and specificity, thereby facilitating the potential application of this approach to more expansive geographical areas.

On the other hand, very few studies focus on the definition of the state of deterioration of AC roofs. Cilia et al. (2015) [14], in a case study in Italy propose an index based on the spectral response in the visible spectrum area (VNIR), relating the state of the cover to the amount of mosses and lichens on its surface. The larger the quantity, the greater the deterioration. Finally, they propose a discriminant value to identify the roofs with high intervention priority for the competent authorities. Spectral measurements in the field served to validate the results obtained with the proposed index. However, mosses and lichens on the roofs are typical of the case study, and it remains to be confirmed if the proposed index it has application in other latitudes of the planet, especially in urban areas of tropical and desert zones. In addition, the study is based on multispectral images, therefore, it would be crucial to investigate its effectiveness with hyperspectral images.

An additional investigation illustrates the efficacy of remote sensing information for the evaluation of degradation in asbestos ceilings [10]. Specifically, the state of the covering material was ascertained through the correlation between the quantified mineral fibers exposed and analysed in both laboratory and field specimens, alongside the spectral reactivity at wavelengths of 2.32 μm and 9.44 μm (Short-Wave Infrared – SWIR and Thermal Infrared - TIR). The researchers seemingly achieve promising outcomes, despite the constraint of a limited field observation and the utilization of multispectral aerial images with ground accuracy of 3 m, in contrast to the hyperspectral imagery employed within laboratory settings.

In light of the aforementioned, a notable dearth of research exists concerning the assessment of degradation states and the establishment of prioritization benchmarks aimed at addressing the conundrum of asbestos roof deterioration and priority intervention. The utilization of hyperspectral imagery for such investigations remains infrequent, as well as for works conducted in tropical and arid urban areas, where climatic factors may influence outcomes. Furthermore, it is pertinent to underscore the significance of this matter, which is poised to retain its prominence over the forthcoming decades, particularly within developing nations that have recently enforced bans on asbestos or are currently in the process of doing so. It is noteworthy that merely 70 out of the world's 200-plus countries have prohibited asbestos, underscoring the global relevance of this issue [18].

Colombia, recently forbidden asbestos use, exploitation and commercialization, giving authorities five years to legislate in the matter [19]. The first step toward the mitigation of asbestos related environmental and human problems is the asbestos identification. The present work focuses on the urban area of Cartagena de Indias. It is a historical city located on the Caribbean coast of Colombia, known for its colonial architecture. The city is UNESCO cultural heritage since 1984 [20]. However, the city is also facing a significant environmental and public health challenge due to the extensive use of asbestos-containing materials.

This manuscript presents an innovative approach for the detection of asbestos-cement roofs within urban context, employing hyperspectral data acquired from airborne platforms. The primary objective of this methodology is to assess the priority level of intervention of these roofs and provide a tool to governmental bodies for the prioritization of intervention and mitigation measures. Four distinct methodologies, encompassing three novel techniques, were implemented, and subjected to comparative analysis to identify the degradation status of asbestos-cement roofs in expansive urban zones. The validation of results was conducted through the establishment of control points in the field, affirming the effectiveness of both the classification process and the prioritization of intervention strategies.

2. Methodology

The workflow of the present investigation will be elucidated within the current section and visually depicted in Fig. 1.

2.1. Case of study and field sampling campaign

The study area encompasses the urban zone of Cartagena de Indias, located in northern Colombia, with a population of approximately 1 million people and covering an area of 80.9 square kilometers (Fig. 2). The city is marked by a dense concentration of residential areas, a limited presence of green spaces between urban areas, and a lack of coherent urban planning, which is a typical situation in developing countries [21].

In a field campaign were randomly collected 215 roof samples of 1 cm × 1 cm with variable thickness between 4 mm and 7 mm in the study area. The samples were analysed with a polarized light microscopy (PLM) according to the EPA 600/R-04/004 International Standard, using a Leica DM750P microscope. Asbestos fibers, fibers type and fiber/cement matrix percentage were analysed. Additionally, 20 samples of 15 cm × 40 cm of roof were taken to carry out laboratory tests with hyperspectral sensors. For the visible and near-infrared range was used the Hyspex VNIR-1600 sensor with 160 bands each 3.5 nm, from 400 to 1000 nm. On the other hand, HySpex SWIR-320e sensor with 256 bands each 6.25 nm, from 1000 to 2500 nm was used for the short-wave infrared (SWIR). These laboratory tests were carried out in a controlled light environment with halogen lamps to simulate the ultraviolet rays emitted by the sun.

2.2. Hyperspectral data acquisition

The acquisition of hyperspectral imagery was executed through an aerial survey employing the Mjolnir VS-620 sensor, manufactured by HySpex, and facilitated by BlackSquare Colombia. This advanced sensor possesses the capability to capture wavelength information spanning from 400 nm to 2500 nm, distributed across 490 spectral bands. Specifically, it encompasses 200 bands in the visible spectrum with a spectral interval of approximately 3.0 nm, and 290 bands in the short-wave infrared (SWIR) spectrum with a spectral interval of about 5.1 nm, [22].

The aerial survey was conducted over a three-day period utilizing a Cessna TU206F Turbo aircraft, covering the geographical expanse of Cartagena. The survey duration took into account intermittent interruptions due to air traffic congestion, primarily resulting from the proximity of an international airport within Cartagena's urban vicinity. The flight plan, illustrated in Fig. 3, was executed at an altitude of 800 m. Consequently, the coupled Mjolnir sensor exhibited a ground coverage width of 250 m for each imaging line, aligned with the requirements of the flight plan. To ensure comprehensive data capture and prevent potential data loss within each line, a 25% overlap between capture lines was maintained. Following data acquisition, the obtained images underwent rigorous radiometric, geometric, and atmospheric corrections. These corrective measures were applied utilizing the HySpex RAD, Rese PARGE, and Rese DROACOR software tools, respectively.

2.3. Roof classification

The processing of hyperspectral images was conducted using ENVI® Version 5.6 software. Initially, data sets were readied for classification, alongside the prior steps of orthorectification and atmospheric correction. To enhance processing efficiency, noisy bands were excluded based on visual assessment, followed by resampling of pixel dimensions from 0.4 m to 0.8 m to mitigate computational load while retaining data integrity.

The Minimum Noise Fraction (MNF) method is a widely recognized approach employed in the realm of hyperspectral imagery denoising. This technique effectively converts a noisy data cube into a set of output channel images characterized by progressively escalating levels of noise [23]. According to the literature [24,25], MNF used in the case study to reduce the size of the dataset, extract the noise from the images and improve the quality of the information.

Subsequently, the first components that contained the best signal to noise ratio were extracted and used to calculate the Inverse MNF in order to obtain the image again in reflectance values, with less noise, [26]. On the other hand, a layer of the of built-up areas of the city was created to avoid burden the process with roads, green areas and bodies of water present in the city.

2.3.1. Classification performance metrics

The supervised classification was carried out with the SAM algorithm (ENVI®). Part of the asbestos-cement (AC) roofs positively identified with PLM analysis were used as training points (10 pixels, equivalent to 0.8 m × 0.8 m), while the others were used to validate the results obtained (139). Following the completion of classification, a confusion matrix is typically generated to delineate

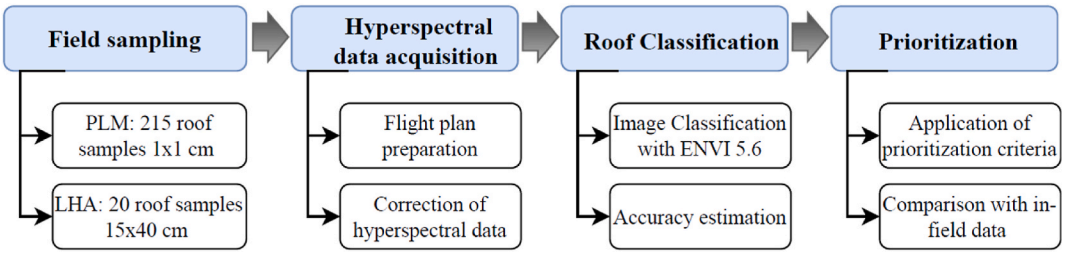

Fig. 1. Methodology workflow. PLM= Polarized Light Microscopy; LHA = Laboratory Hyperspectral Acquisition.

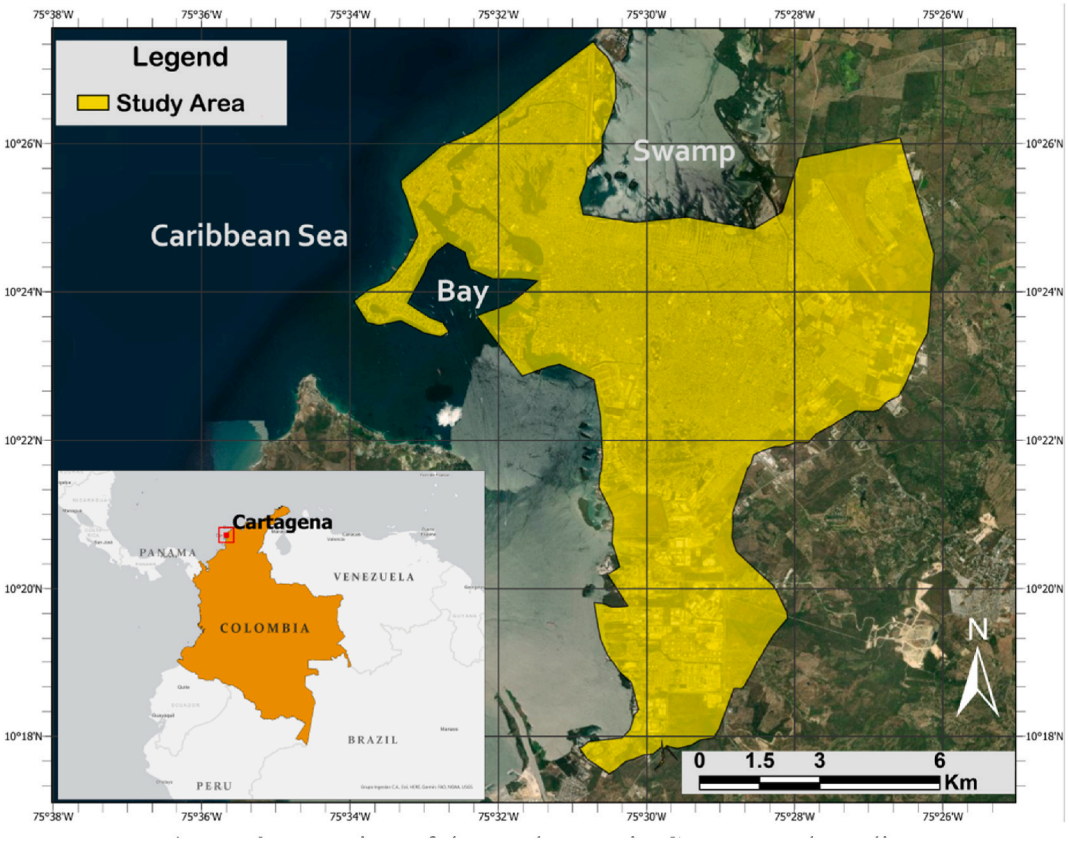

Fig. 2. Location of the study area in Cartagena de Indias.

the classification's quality [17,27]. The confusion matrix defines errors in the classified image relative to the ground truth. Essentially, two distinct types of errors manifest: the omission error, representing the likelihood that a classified pixel aligns with the ground truth, and the commission error, denoting the probability that a pixel classified within a specific class genuinely pertains to that class (1–4).

$$Producer\ Acuracy = \frac{TP}{TP + TN} = \frac{TP}{Total\ Referenced} \tag{1}$$

$$Ommission\ error = 1 - \ Producer\ Acuracy \tag{2}$$

$$User\ Acuracy = \frac{TP}{TP + FN} = \frac{TP}{Total\ Predicted} \tag{3}$$

$$Commission\ error = 1 - \ User\ Acuracy \tag{4}$$

where TP is the number of True Positives in a class, FN is the number of False Negatives and TN is the True Negatives. These metrics were computed for the most common roof classes distributed across the study area. Conversely, Overall Accuracy (OA) was determined as the proportion of accurate predictions relative to the total number of predictions, computed by dividing the sum of the diagonal elements in the confusion matrix by the total number of predictions.

The final classification was exported to the ArcGIS® software for post-processing in Geographic Information Systems (GIS).

2.4. Characterization of roof deterioration state

Among the roofs selected in the field, those that showed the presence of asbestos to PLM, were assessed in field to define their state of deterioration, discriminating between High Intervention Priority (HIP) and Low Intervention Priority (LIP) [14]. These priority levels refer to the need or not to urgently intervene in the asbestos-cement roofs, either through radical measures such as the removal of AC, or through mitigation methods such as enclosure or encapsulation [28–32]. The method used in the field to differentiate between HIP and LIP is the traditional method of visual qualitative inspection [33,34]. Table 1 shows the parameters considered in the present research, similarly to other methodologies found in literature [35,36]. Therefore, when one or more parameters of deterioration are widespread (general) on the surface of the roof, it is considered a HIP due to the high probability of releasing asbestos fibers into the

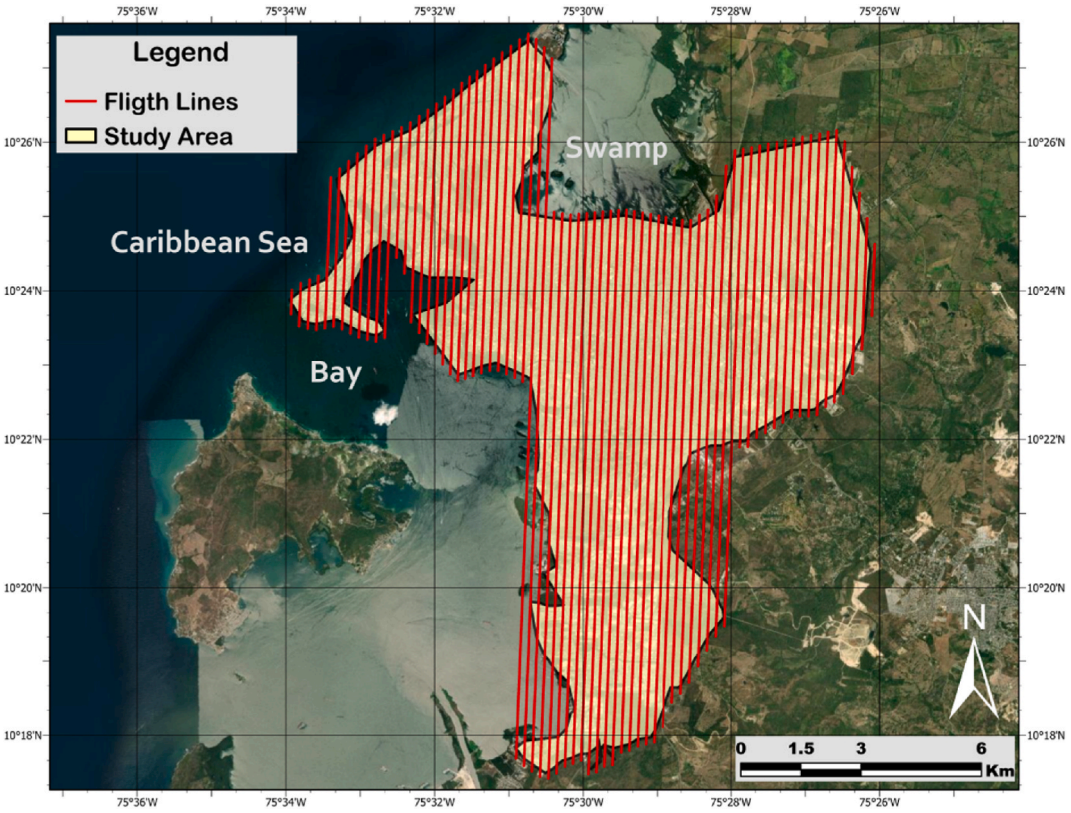

Fig. 3. Planned flight plan.

environment [10,37]. In other cases, the local or absent deterioration will classify AC roofs as LIP.

However, this methodology would be difficult to apply in large urban areas with a high presence of AC roofs. Furthermore, these tools alone are not useful for decision-making authorities to optimize strategies and resources to mitigate asbestos contamination, especially in developing countries.

On the other hand, the present research applies four discrete methodologies to delineate the extent of degradation in AC roofs through remote sensing. The proposed indices will be applied on hyperspectral data to the roofs analysed in the field positive for the presence of asbestos. This will allow to establish LIP and HIP according to remote sensing data. The comparison between the results on field analysis and the results of the four discrete methodologies coming from remote sensing data will allow to establish the accuracy of the planted methodology for large scale application.

The first method is grounded in prior literature [14], whereas the subsequent trio of methods are introduced by the researchers as innovative components within the current study.

Drawing from existing literature [14],a spectral indicator known as the Index of Surface Deterioration (ISD) was applied (5). This indicator, unlike its direct linkage to surfacing fibers, is intricately associated with the heightened presence of mosses and lichens on the top part of the asbestos-cement-roofs. These growths have been documented to exhibit greater prevalence on older asbestos-cement external sheets in Italy. The spectral index considers the absorption profiles of photosynthetic pigments found in vegetation, as well as the inherent color of the asbestos-cement (AC), which generally darkens as roofs undergo weathering. The formulation of the spectral index is presented below (5).

Table 1
Parameters to define intervention priority through qualitative in field observations.

	Distribution on the top roof surface		
Roof Parameters	General	Local	Absent
Black, moss, vegetation cape	–	–	–
Cracks, fissures or holes	–	–	–
Poor state of the edges	–	–	–
Surface release of fibers by hand	–	–	–
Friable matrix	–	–	–

$$ISD_{Veg} = \frac{CR_{680}}{R_{740}} \quad (5)$$

Delving into specifics, the subscript Veg refers to vegetation, to generally state mosses and lichens, $CR_{0.68}$ signifies the Continuum-Removed reflectance value at 680 nm, a wavelength coinciding with the nearest Hyperspectral band to the chlorophyll absorption peak (600–700 nm) [38–40]. Conversely, $R_{0.74}$ denotes the reflectance observed at 740 nm, a measurement accounting for the luminosity of the cement matrix, which turns out to be the positive reflectance peak immediately to the right of the vegetation absorption peak. The technique of continuum removal serves as a mechanism for quantifying absorption characteristics at precise wavelengths, standardizing reflectance spectra against a shared baseline [41]. This procedure involves the application of continuum removal, wherein the continuum is approximated through linear segments connecting local spectral maxima. Under this approximation, local maxima are attributed a value of 1, while values between 0 and 1 correspond to absorption features. To construct the continuum baseline and calculate the depth of the chlorophyll absorption feature at 680 nm, reflectance data was interpolated between bands centered at 0.60 and 740 nm. This method is therefore based on Visible and Near-Infrared (VNIR) spectral data.

Following a similar path, the authors propose an alternative spectral index (6), based on short-wave infrared (SWIR) bands (as observed in Fig. 4) and chrysotile absorption peak between 2300 and 2350 nm).

$$ISD_{2327} = \frac{CR_{2327}}{R_{2387}} \quad (6)$$

where CR_{2327} represents the average value of Continuum-Removed reflectance measured between 2326 and 2331 nm, where the bands are absorbed by chrysotile [10], R_{2387} designates the reflectance recorded at 2387 nm for the asbestos-cement matrix, in correspondence to the pure cement reflectance peak. This distinction arises from the documented observation that the spectral characteristics of asbestos-cement, in the SWIR segment of the spectra, fall always above pure chrysotile spectra and below the cement spectral signature.

A third index is proposed (7), focused on the reflectance of the absorption peak at 2327 nm, which is a characteristic peak for chrysotile, cement and asbestos-cement material.

$$ISD_{CAP} = \frac{R_{Sample2327} - R_{Chry2327}}{R_{Cem2327} - R_{Chry2327}} \quad (7)$$

where CAP means Chrysotile Absorption Peak, R_{2327} represents the reflectance recorded at 2327 nm for the asbestos-cement sample ($R_{Sample2327}$), chrysotile ($R_{Chry2327} = 0.111$) and cement matrix ($R_{Cem2327} = 0.353$).

The fourth method proposed for the intervention priority is based only on the asbestos-cement sample reflectance at 2327 nm (R_{2327}).

The iterative assessment of the four intervention prioritization indicators in relation to the field-derived prioritization data (Table 1) enabled the reduction of predictive discrepancies and the determination of optimal values for each indicator.

3. Results and discussion

A total of 215 specimens acquired from rooftop evaluations conducted in the field were subjected to analysis utilizing polarized light microscopy (PLM). The results reveal that 188 of these specimens exhibited the presence of asbestos-chrysotile, with a volumetric ratio relative to cement of 38.73 ± 8.10%. In 52 of these cases, a concurrent presence of crocidolite was discernible, with a volumetric

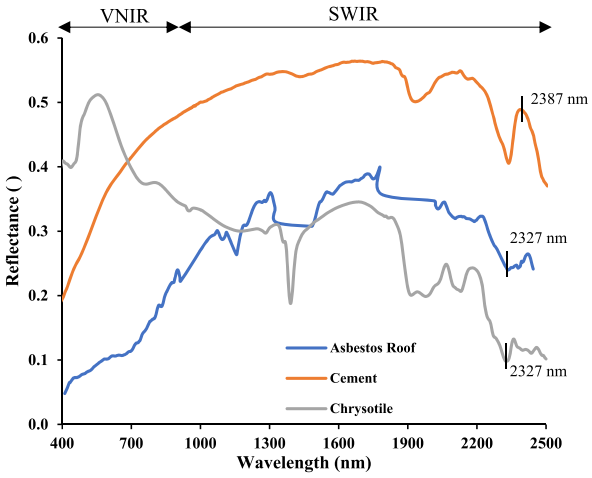

Fig. 4. Typical spectral signature for cement (taken from Ref. [42]), chrysotile (taken from Ref. [43]) and asbestos-cement roofs (taken from Ref. [6]). ( ) = non-dimensional.

ratio relative to cement of 10.83 ± 6.06%. Notably, only one specimen exhibited the coexistence of amosite (as detailed in Annex 1). In 64 samples, a concurrent presence of cellulose was found with chrysotile with a volumetric ratio relative to cement of 6.25 ± 3.92%.

The remaining 27 samples consisted of fiber-cement material asbestos-free, typically representing recently installed roofs. In this samples a significantly higher presence of cellulose was found, 30.6 ± 6.08% volumetric ratio relative to cement. According to the literature [44–46] cellulose is commonly found in asbestos-cement tiles due to its roles in enhancing structural strength, preventing cracks during tile production, and ensuring dimensional stability. However, asbestos-free fiber cement tiles have a higher cellulose content, around 30%, mainly because of evolving safety regulations and health concerns related to asbestos. To replace asbestos, manufacturers used cellulose fibers, among others, which provide structural benefits and are safe. The increased cellulose content in these tiles maintains their desired properties without relying on hazardous asbestos, aligning with modern safety and environmental standards.

The PLM observations illustrating asbestos presence in a representative sample are visually presented in Fig. 5(a–d).

The image analysis conducted on asbestos-cement via Polarized Light Microscopy (PLM) revealed distinct characteristics. Specifically, the photograph captured crocidolite and chrysotile asbestos fibers from a roof sample at 40× magnification under plane-polarized light. Notably, the crocidolite asbestos fiber-bundles displayed a blue-gray pleochroism with high relief, while the chrysotile appeared nearly invisible (low relief) when immersed in a 1.550 HD refractive index liquid. Additionally, non-fibrous components exhibited optical properties consistent with carbonates and other minerals commonly found in concrete cement. It is essential to highlight that both types of asbestos were abundant, highly asbestiform, and easily detachable from the substrate.

In terms of the imaging technique, plane-polarized light was employed to emphasize the crocidolite pleochroism, where the blue hue ran parallel and the gray hue perpendicular to the primary vibration direction of the microscope. When using crossed polars, a predominantly black background was observed, with crystals exhibiting first-order interference colors. Notably, due to the use of a 1.550 high dispersion refractive index liquid, the chrysotile, although low in contrast, displayed a heightened birefringence, rendering it brilliantly white against the black background.

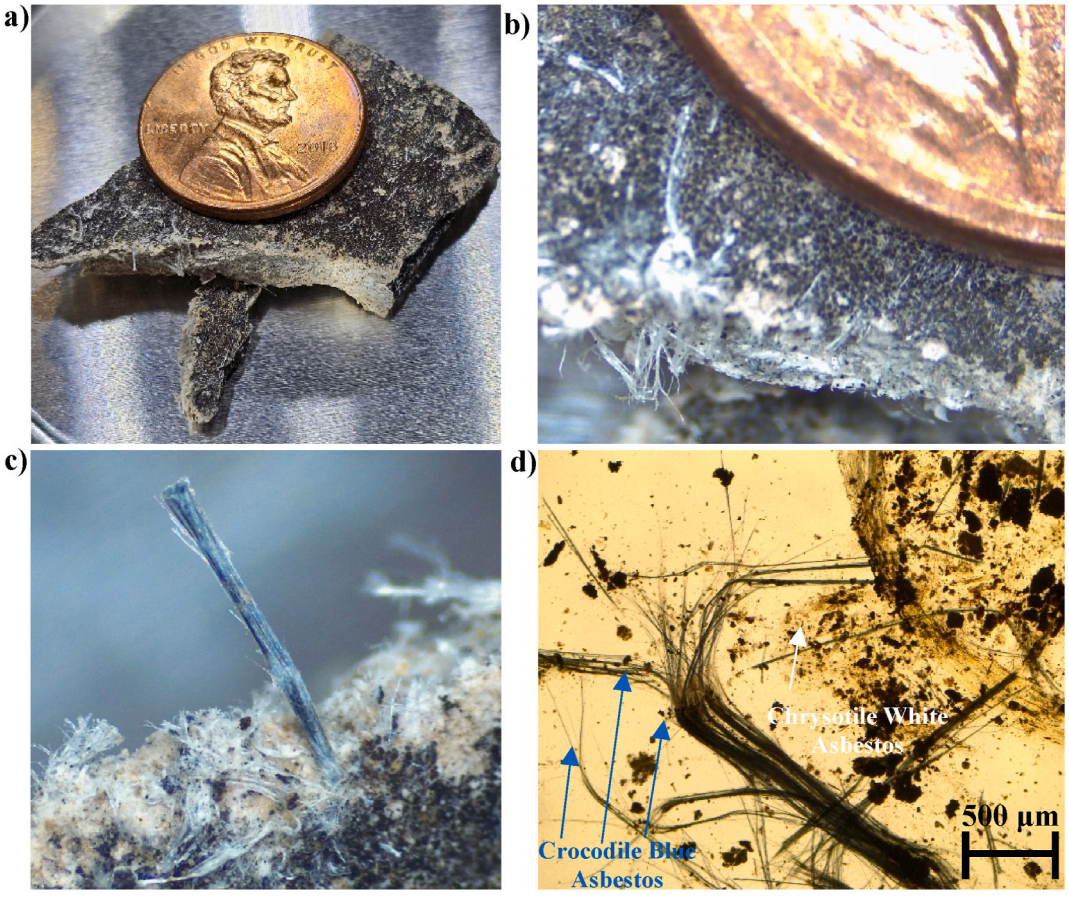

Fig. 5. (a) Roof top Asbestos-Cement sample; (b) a detailed view of the sample; (c) visible blue and white asbestos fibers: d) Crocidolite and Chrysotile asbestos from a roof sample. Photograph taken under polarized light microscopy (PLM) at 40× magnification; plane-polarized light. (For interpretation of the references to color in this figure legend, the reader is referred to the Web version of this article.)

3.1. Asbestos-cement roof classification

Fig. 6 illustrates the impact of atmospheric correction on the spectral signature, revealing the attainment of a uniform spectral profile that more accurately mirrors the characteristics of AC materials.

Additionally, the application of noise calculations using the Minimum Noise Fraction (MNF) tool enhances the spectral signature, particularly in regions characterized by low spectral signal, such as the Short-Wave Infrared (SWIR) zone and areas within the spectrum surrounding the atmospheric windows at approximately 1000 nm, 1300 nm and 1900 nm.

Fig. 7 shows the results of the hyperspectral classification of asbestos roofs in the urban area of Cartagena de Indias. The absence of hyperspectral data within the central zone represents the 11.4% of the total study area. It is related to the prohibition to overflight approach cone the Cartagena's international airport of for security reasons. Within this sector, adherence to the designated ceiling of 800 m for aerial surveys has not been feasible, resulting in a data-deficient zone. Hence, it is imperative to document this instance to prompt forthcoming investigations to factor in such contingencies. Accordingly, strategies must be formulated to augment the dataset through the integration of satellite imagery and alternate methodologies geared towards identifying asbestos-cement roofs within vicinities encompassing airports or other critical infrastructural installations.

On the other hand, results show a widespread use of AC roofs in the city. In the 190 neighbourhoods of Cartagena, the present research found an average AC roof area of 20.4% over the total area of the neighborhood, with neighbourhoods that have a peak of more than 47.6% of their total area covered by AC roofs. A total of 9.1 km^2 of AC roofs were identified in the city of Cartagena representing the 11.2% of the total study area. Given that the region lacking hyperspectral data defines as landing cone, urban planning and stratification attributes are entirely analogous to the remainder of the city, it could be inferred the potential existence of an additional 2 km^2 of asbestos-cement (AC) roofing. This estimate is based on maintaining a consistent average with the broader city context. This is an astonishing amount that should raise alarms for the competent authorities, academic and general community. Despite a marked social difference in the city and a profoundly different urban planning depending on the sector, small differences are noted in the identified quantities of AC between neighbourhoods of high and low social strata. Even in the historic centre, a UNESCO heritage site and in the tourist area (extreme north-west of the city in Fig. 7 (a - c), the presence of AC roofs represents up to 13% of the total neighbourhoods area [6].

Of the 188 roof samples asbestos positive to PLM analysis, 149 resulted in the area from which hyperspectral information could be collected. Therefore, in the assessment of classification quality, attention is directed toward the analysis of accuracy in the classified image vis-à-vis the ground truth. Noteworthy is the producer accuracy score of 98%, signifying a high probability of a classified roof aligning with ground truth, thus indicating the accurate classification of 146 out of the total 149 roofs. Conversely, an overall accuracy of 96% is observed, representing the ratio of correctly classified roofs to the total number of ground truth roofs, including non-asbestos-cement roofs (Tables 2 and 3).

These results underscore a heightened precision in the discrimination of asbestos roofing materials from alternative roofing materials, a pattern consistent with the most accurate findings in existing scientific literature in the matter [10,13–15,24,47,48]. However, it is important to note that such findings in literature are often limited to smaller spatial scopes and encompass fewer instances within the ground truth dataset. Additionally, it is pertinent to acknowledge the lack of literature addressing densely populated urban centers in developing nations, which are typically characterized by diminutive residential structures with roofs covering less than 30–40 m^2, representing a further challenge.

Fig. 8 shows two typical classification errors in the case study. In one case (Fig. 8a–b), the asbestos-cement roof of a school is observed with a high density of trees around it, which generate a shadow on the roof, additionally releasing a high amount of leaves on top of the roof. Therefore, in the parts covered by the shadow, the misclassified pixels are partly confused with other pixels. It is common to find in literature classification errors generated by the roof inclination, shadows of trees, clouds, and other buildings

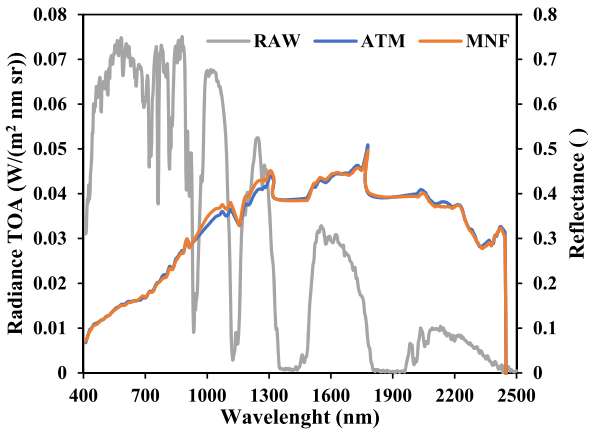

Fig. 6. Spectral signature of AC material: Raw (vertical axes indicates Radiance Top of Atmosphere (TOA)); Spectral signature after Atmospheric Correction (ATM) and after MNF correction. Vertical axis for ATM and MNF is Reflectance. ( ) = non-dimensional.

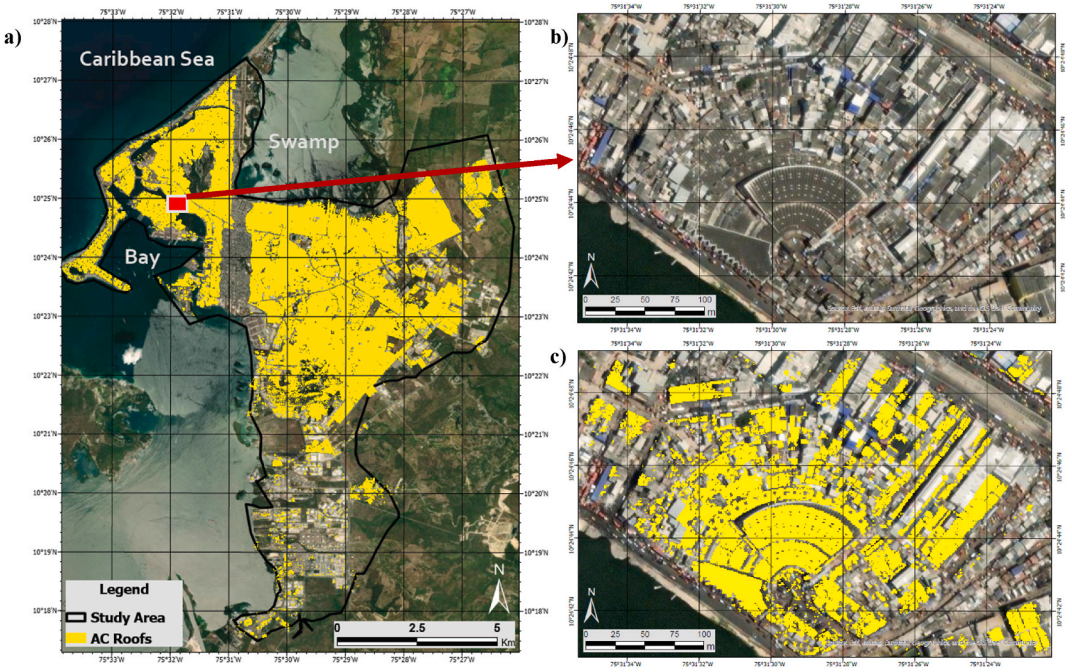

Fig. 7. (a) Asbestos-cement roofs identified in the study area; (b) a section of the city in the public market before the identification of asbestos-cement; (c) identification of asbestos-cement roofs in the public market shown above. The area is characterized by a confusing urban organization; however, the roofs are well identified.

Table 2
Confusion Matrix based on typical roofs in the study area (clay, steel, and AC roofs).

Confusion Matrix					
		Ground Truth			Total Classified
		Clay	Steel	AC	
Classification	**Clay**	**47**	1	2	50
	Steel	2	**47**	1	50
	AC	3	0	**136**	139
	Total Ground Truth	52	48	139	**239**

Table 3
Classification accuracy.

	Clay	Steel	AC
User Accuracy	94%	94%	98%
Commission error	**6%**	**6%**	**2%**
Producer accuracy	**90%**	**98%**	**98%**
Omission error	10%	2%	2%

[13–15,24,47]. Furthermore, in large areas, as in the case study, where the hyperspectral acquisition is carried out during different days and at different times, the presence of clouds and different degrees of shadow is almost inevitable.

In the second case (Fig. 8 c-d), it is a specific case, since between the moment in which the sample was taken in the field and the moment in which the hyperspectral flyby was carried out (15 days difference), the cover was replaced with a cover in steel. Therefore, this cannot be fully considered a classifier error. These cases are unpredictable and can happen frequently in very dynamic realities such as developing countries.

Furthermore, in the literature unclassified roofs often exhibit surface alterations such as painting or treatment with specialized products that engender modifications in their spectral profiles as shown by Frassy et al. (2015) [7]. The present study encountered analogous difficulties in accurately identifying painted asbestos roofs, attributed to the distinct spectral contributions stemming from compositional modifications. These findings underscore the imperative for supplementary methodologies and data sources to enhance the precision of classification outcomes.

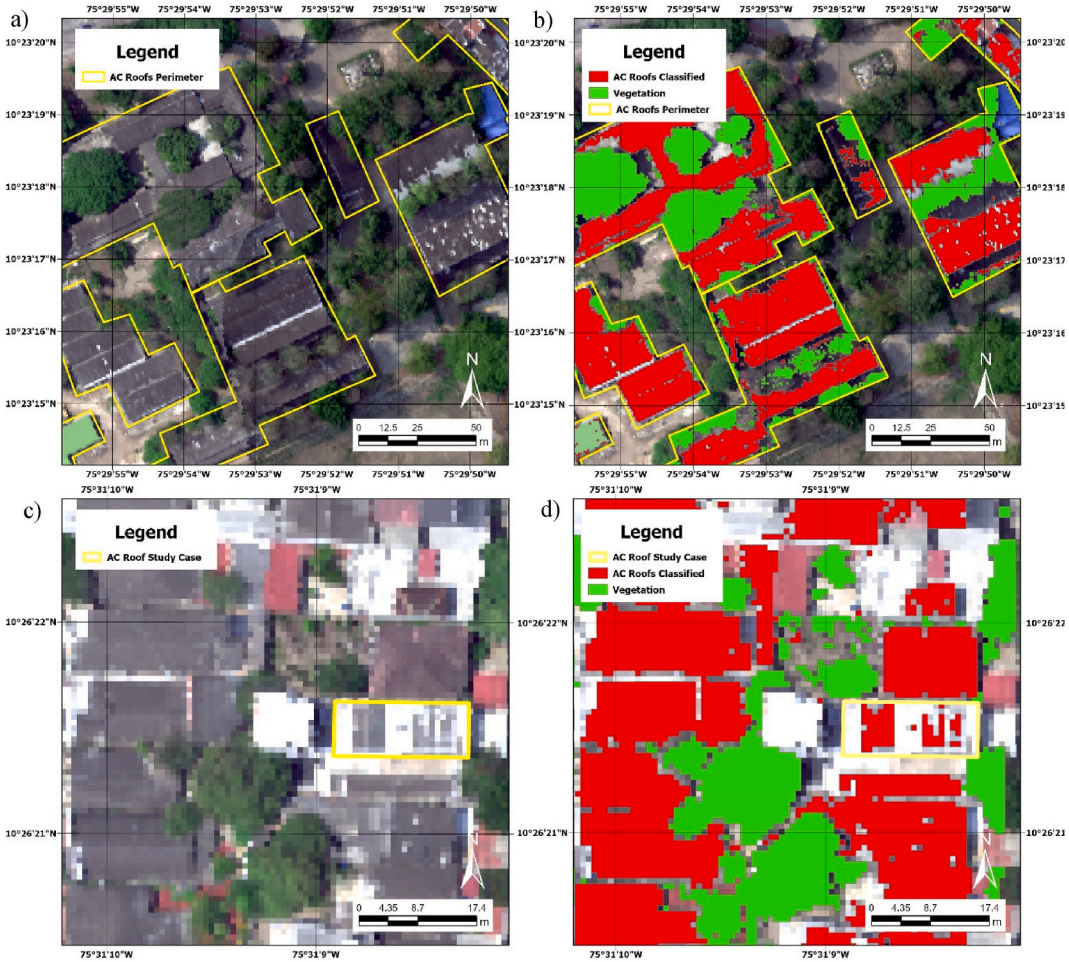

Fig. 8. Examples of typical classification errors: (a) image before and (b) after classification asbestos-cement roof of a school is observed with a high density of trees; (c) and (d) image of an AC roof partially replaced with steel.

Finally, as previously indicated, the examination of hyperspectral signatures pertaining to roofs identified the prevalence of two predominant materials distinct from asbestos-cement, namely clay and steel roofs. The spectral characteristics of these materials align with documented findings in the scientific literature [49] (Fig. 9).

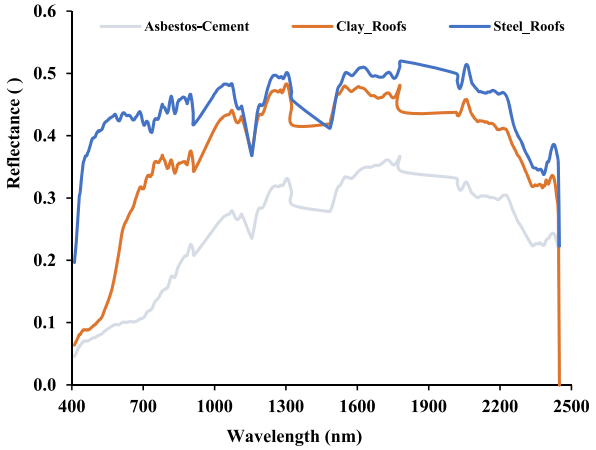

Fig. 9. Most common spectral signatures found in the study area. ( ) = non-dimensional.

3.2. Prioritization of intervention in asbestos-cement roofs

The delineation of intervention prioritization for asbestos-cement roofs, categorized as lower and higher priority, holds noteworthy significance for competent regulatory bodies and governmental entities. Especially, within developing nations or those actively engaged in the cessation of asbestos usage and the formulation of legislation to ameliorate its detrimental impact on human well-being. This is particularly pertinent in cases where substantial asbestos quantities coexist with limited resources for incentivizing the eradication of this hazardous substance. The strategic prioritization serves as a pivotal approach to optimize outcomes.

Field assessments revealed that among the 149 AC roofs examined, 24 were categorized as having low intervention priority (LIP), accounting for 16.1% of the total, whereas 125 were designated as high intervention priority (HIP), constituting 83.9% of the total. This disparity is understandable since most of the roofs have been installed for more than 30 years and have endured weathering and interventions. Taking the spectral signature of the LIP and HIP roofs and plotting them separately as an average with a 90% confidence interval (CI), it was identified that there is a certain tendency for the HIP roofs to have higher reflectance than the LIP roofs (Fig. 10 (a–b)). As explained in the methodology, it is noted that all the spectral signatures of the AC roofs are between the spectral signature of the cement and the chrysotile, especially in the SWIR part after 1900 nm, confirming what is found in the literature [10].

In the aforementioned SWIR part, it is evident that AC covers in good condition (LIP) have a spectral signature closer to chrysotile. This is probably due to less weathering and greater presence of chrysotile in the cover. On the other hand, roofs classified as HIP present the opposite behaviour, probably due to a great persistence of asbestos fibre over the years. In support of this, it is demonstrated in the literature [10,37,50] that AC covers can lose up to 3 g of asbestos fibers per m^3 per year, generating significant surface deterioration, compromising the state of the compact matrix.

Given the marked disparity between LIP and HIP data in the field, the authors generated 101 synthetic spectral signatures for LIP, while preserving their mean and standard deviation. This procedure was undertaken to balance the quantities of LIP and HIP spectra. The primary aim of this methodology was to empirically examine the performance of the prescribed Prioritization Methods (namely, ISD_{Veg}, ISD_{2327}, ISD_{CAP} and R_{2327}) utilizing a combination of authentic and synthetic data derived from hyperspectral imagery (Fig. 11 (a - d)). Furthermore, the study sought to establish a comparative analysis against qualitative data gathered through on-site field assessments concerning the prioritization of interventions.

To assess the accuracy of the proposed methods, a statistical analysis was carried out with and without synthetic data. The limit value of each method was determined with the objective of optimizing the precision in the determination of the LIP and HIP roofs between hyperspectral data and qualitative field data (Fig. 12(a–d)).

Table 4 shows the optimal values found for each method and its corresponding optimal precision value. Several considerations can be made about the above. Primarily, it is observed that the ISD_{680} index proposed by Cilia [14], which discriminates as >4 HIP and <4 LIP, in the case of Cartagena does not apply because for that value there are errors of up to 96% in predicting the level of intervention of a roof in field through the proposed index. However, it has been noted that the optimal value of this index for the case study is between 5.17 and 5.22 with precisions that do not exceed 40% even decreasing when introducing synthetic LIP data. The values of this index for

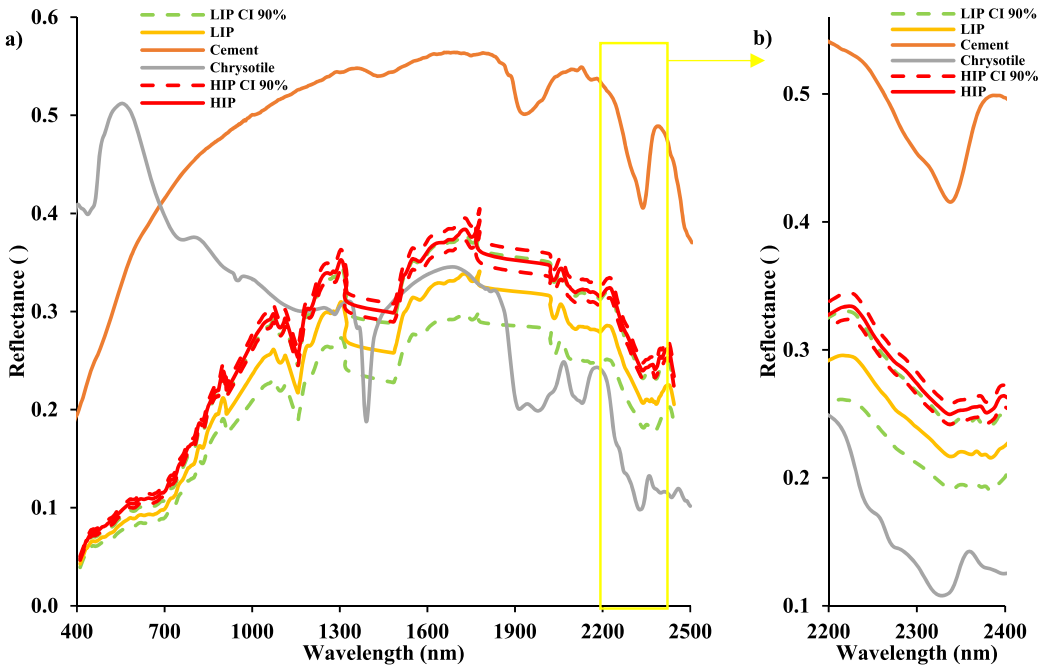

Fig. 10. (a) Average spectral signature of HIP= High Intervention Priority and LIP = Low Intervention Priority roofs of the case study no synthetic data included; (b) zoom of the chrysotile, cement, and asbestos-cement (AC) absorption peak around 2327 nm and CI curves. ( ) = non-dimensional.

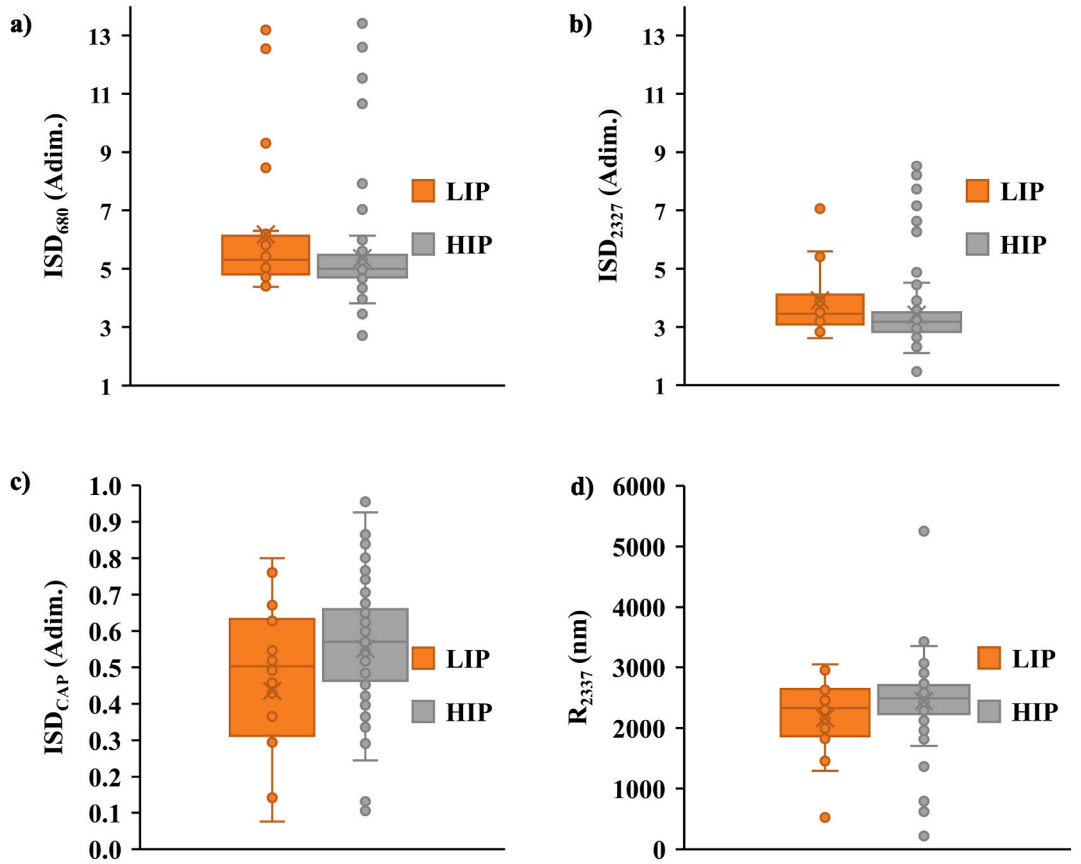

Fig. 11. Variation of the values of the indicators of LIP and HIP without synthetic data for each method. (a) ISD_{680}; (b) ISD_{2327}; (c) ISD_{CAP}; (d) R_{2337}.

LIP are on average higher than for HIP covers. Therefore, its sensitivity is not appropriate to the case of Cartagena. This is probably because in a tropical semi-desert area like the study area, there is no such pattern of grown vegetation, mold and chlorophyll above the covers. Similar results are found for the ISD_{2327}, which is basically a similar index applied to the chrysotile absorption peak. This seems to mean that the formulation of the index is not appropriate even if it applies to other areas of the AC response spectrum.

On the contrary, encouraging results are found for the ISD_{CAP} and R_{2327} both based on the chrysotile reflectance. In the first case, the index considers the spectral range between chrysotile and cement in correspondence of an absorption peak that both materials have around 2327 nm (Fig. 10 b). In the second, only the reflectance at that same wavelength is considered. Both proposed methods seem to have a high precision, around 60%, with an increase up to 70% when the method is fit with the synthetic LIP data.

However, the errors remain significant, also with these last two methods proposed by the authors. This is probably because it is compared the state of an asbestos-cement roof and its level of intervention on the one hand with a qualitative analysis in the field, results of a visual analysis, and on the other with hyperspectral data that do not consider factors such as small cracks, fissures or holes, poor condition of the edges, superficial release of fibers by hand among other factors. Furthermore, it must be considered that the AC roofs analysed show different percentage contents of chrysotile fibers, depending on the producer and the production period. Other types of asbestos fibers (crocidolite and amosite) mixed in different percentages with chrysotile have also been found in some samples (annex 1), which may reduce accuracy since they have a different spectral signature as shown in literature [51].

The innovative aspect of this study lies in the introduction of a tool with a commendable level of reliability, particularly the ISD_{CAP} and R_{2327} methodologies, which are highly valuable in extensive urban environments characterized by a substantial concentration of AC roofs. Such environments necessitate the development of effective intervention and prioritization strategies. The significance of tools of this nature cannot be overstated, particularly in developing nations where knowledge in this domain is limited, urban areas witness pronounced AC proliferation, environmental awareness remains nascent and economical resources are limited. It is worth noting that a substantial portion of the global population, numbering at least one billion individuals, one-sixth of the Earth's population, resides within the confines of subtropical desert regions [52], predominantly within developing nations that share characteristics akin to those observed in the study area. Consequently, the findings of this research hold potential applicability to tens of thousands of analogous cities worldwide.

On the other hand, a comparison is proposed between the four methods with data from hyperspectral laboratory tests and hyperspectral sensors used for the overflight, in the same roofs. It was calculated the percentage error of each series of coordinates by comparing the actual values with the values predicted by the linear equation ($y = x$) (Fig. 13(a–d)). A trend consistent with Fig. 12 and

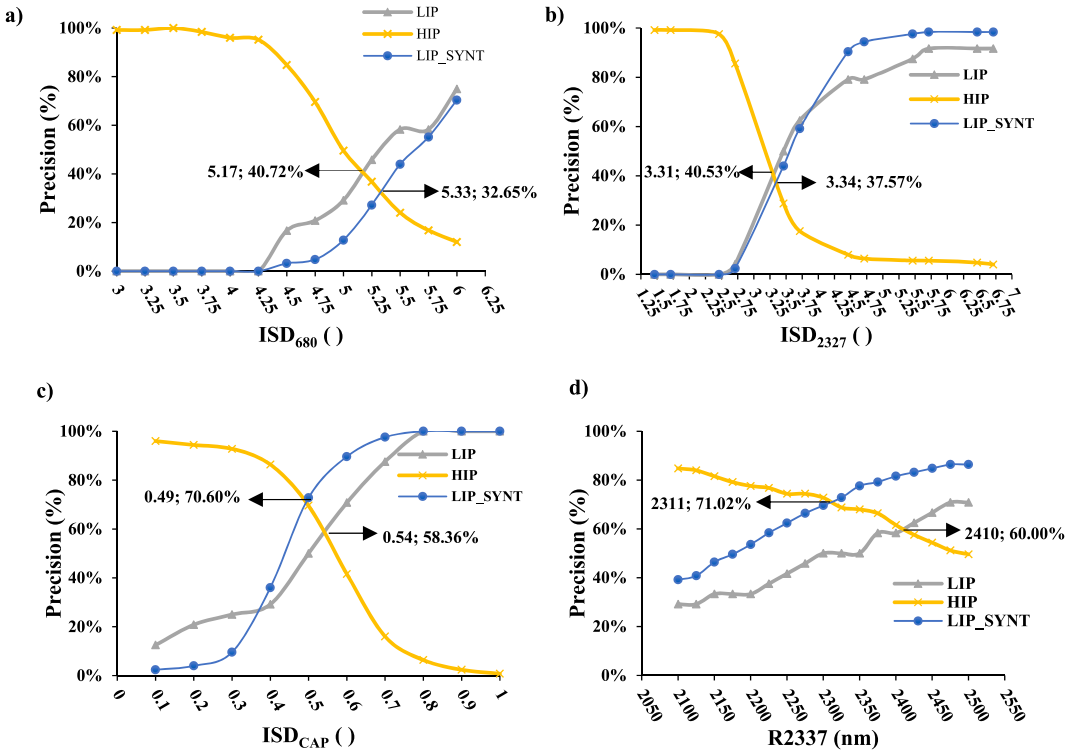

Fig. 12. Assessing the fluctuation in the precision of each method for the identification of Low Intervention Priority (LIP) and High Intervention Priority roofs (HIP), both with and without the inclusion of synthetic data (SYNT). (a) ISD_{680}; (b) ISD_{2327}; (c) ISD_{CAP}; (d) R_{2337}.

Table 4
Parameters to define intervention priority through in field observations.

Parameter	Prioritization Methods			
	ISD_{680}	ISD_{2327}	ISD_{CAP}	R_{2337}
Optimal Precision (%)	40.72	40.53	58.36	60.00
Optimal Value	5.17 ( )	3.31 ( )	0.54 ( )	2410 nm
Optimal Precision with synthetic data (%)	32.65	37.57	70.60	71.02
Optimal Value	5.33 ( )	3.34 ( )	0.49 ( )	2311 nm

( ) = non-dimensional.

Table 4 emerges, wherein the method existing in the literature exhibits the highest error (ISD_{Veg} Error = 75 %), while the methods proposed in this study demonstrate significantly lower errors up to 35 % (Fig. 13b–d). Once more, the top-performing approach exclusively relies on reflectance. Nonetheless, it is crucial to acknowledge the limitations of these methods, which may be partially attributed to the presence not only of chrysotile in the cement matrix but also of other asbestos fibers like crocidolite and amosite (annex 1), each having distinct spectral signatures compared to chrysotile, potentially leading to deviations [51]. Additionally, it is noteworthy that the ground pixel size in the hyperspectral image is 0.8 m, whereas in the laboratory, it is a fraction of a millimeter; this disparity may also influence the observed reflectance values.

Finally, applying the R_{2327} method to the study area, was found a 49.54% of LIP roofs and 50.46% of HIP roofs in Cartagena de Indias urban area. This observation highlights the presence of a significant number of deteriorated asbestos-cement (AC) roofs within the city, demanding prioritized interventions that warrant swift action from relevant authorities. Fig. 14(a–c) highlights with photographic images and reference samples with relative spectral signature what the authors classify as HIP and LIP.

Nonetheless, in the present case study (Fig. 15(a, b)), as in the existing literature [14] it is found a tendency to classify roof sections with the most shade, typically attributed to steeper slopes, as being in good condition (LIP). Consequently, meticulous flight planning is imperative to capture hyperspectral images during midday hours, specifically between 11 a.m. and 1 p.m. when the sun attains its zenith, minimizing shadow effects on roof slopes and thereby mitigating potential errors.

4. Conclusions

The goal of the present study was to detect asbestos-cement (AC) roofs using hyperspectral imagery and assess the prioritization of

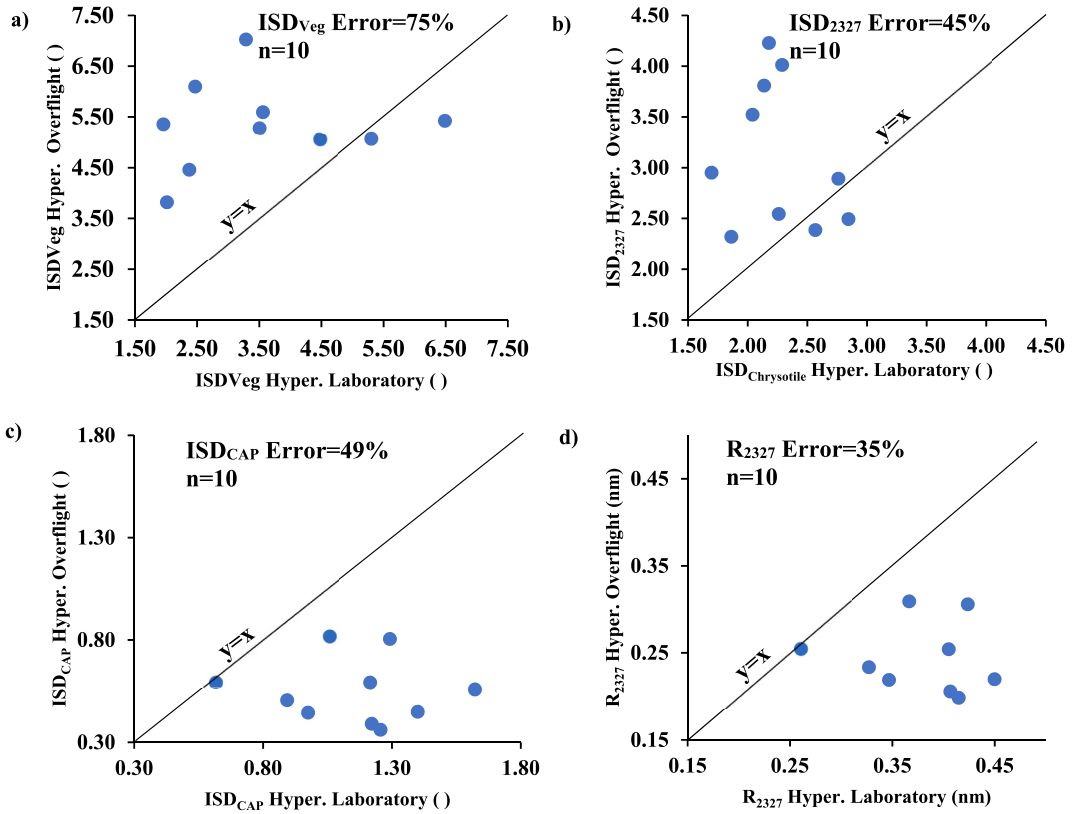

Fig. 13. Comparative error analysis of the four methods proposed, computed in hyperspectral images acquired via aerial overflight and laboratory acquisition. (a) ISD_{680}; (b) ISD_{2327}; (c) ISD_{CAP}; (d) R_{2337}. ( ) = non-dimensional.

intervention measures for AC roofs within an urban scenario. This effort aimed to provide a decision-support tool for governmental bodies in order to streamline the prioritization of interventions and mitigation strategies. Four distinct methodologies, incorporating three innovative techniques, were deployed and subjected to a comparative analysis aimed at discerning between low and high intervention priorities for AC.

Asbestos-cement roof identification shown to be reliable with an overall accuracy of 96% with hyperspectral images, encountering significant amount of AC roofs in the city, 9 million square meters, being AC the most common roof type in the city independent of socioeconomic strata. This shows that it is a transversal problem that affects the entire population and that can have serious consequences on public health in the medium and long term.

Furthermore, results show the new methods proposed to define the intervention priority better fit the case study, and the chlorophyll pattern suggested for the ISD_{Veg} index found in literature is not replicable in tropical desert zones like the case study. More than 50% of the city AC roofs are in critical conditions, high intervention priority (HIP), serving as a compelling call to action, urging regulatory authorities, the wider community, and the academic sphere to collaborate expeditiously in addressing this issue.

The significance of these findings, particularly for developing nations, cannot be overstated. Efficient resource utilization in the management and mitigation of asbestos-containing materials has the potential to significantly reduce the population's exposure to this hazardous element. This, in turn, holds the promise of preserving countless lives and enhancing public health in the decades to come. The far-reaching implications of such improvements extend beyond the realm of healthcare, encompassing multifaceted benefits for society as a whole and the overall economy.

Finally, it is of particular significance to underscore that a considerable segment of the global populace, exceeding one billion individuals, makes their homes within the boundaries of subtropical desert regions. These regions are primarily situated in developing nations that exhibit striking parallels with the conditions observed in the study's focal area. This demographic reality accentuates the far-reaching implications of the present research findings. They not only pertain to the specific context under investigation but also possess a broader relevance that extends to a multitude of analogous urban centers worldwide. The applicability of the present findings transcends geographical boundaries, offering insights and potential solutions that can benefit tens of thousands of cities facing similar challenges and environmental conditions.

Funding

This research was funded by General System of Royalties of Colombia (SGR, for its initials in Spanish) grant number BPIN

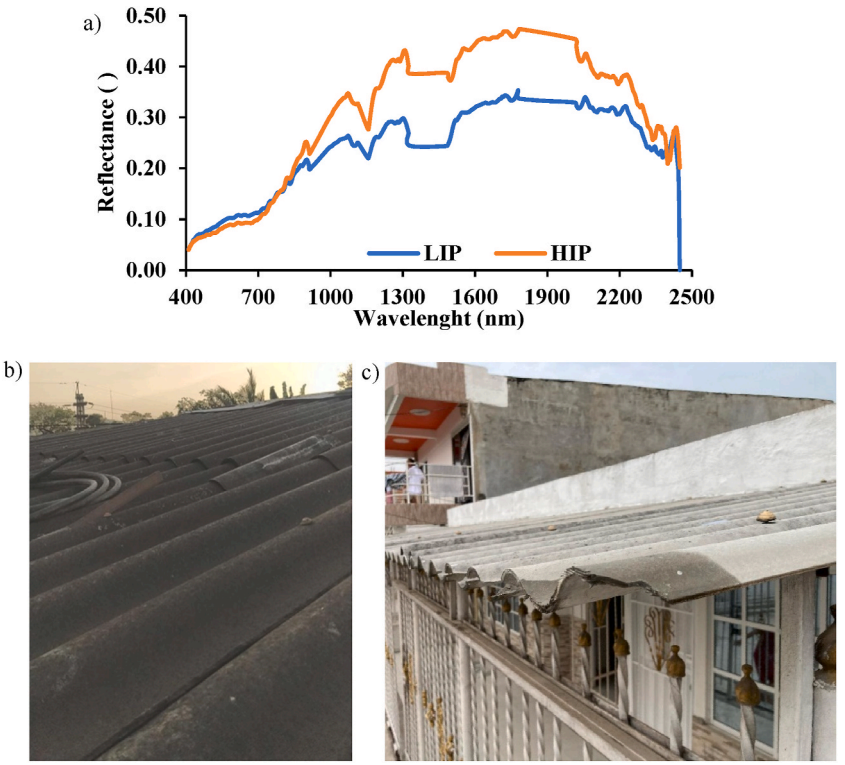

Fig. 14. a) Spectral signature of a typical HIP and LIP roof. Photographic images of reference samples regarding what the authors classify as b) HIP roof and c) LIP roof. ( ) = non-dimensional.

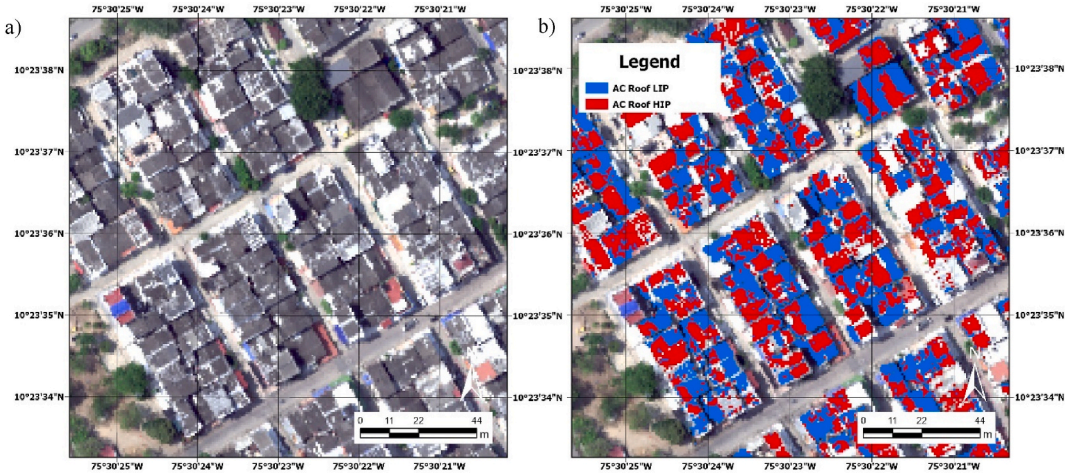

Fig. 15. LIP and HIP classification in the study area with R_{2327} method. a) Unclassified area; b) Classified area.

2020000100366.

Institutional review board statement

Not applicable.

Informed consent statement

Not applicable.

Data availability statement

Data available upon request.

CRediT authorship contribution statement

David Enrique Valdelamar Martínez: Writing – review & editing, Visualization, Resources, Investigation, Formal analysis, Data curation, Conceptualization. **Manuel Saba:** Writing – review & editing, Writing – original draft, Supervision, Resources, Methodology, Investigation, Formal analysis, Conceptualization. **Leydy Karina Torres Gil:** Writing – review & editing, Visualization, Resources, Investigation, Formal analysis, Data curation, Conceptualization.

Declaration of competing interest

The authors declare the following financial interests/personal relationships which may be considered as potential competing interests: Manuel Saba reports financial support was provided by Colombian General System of Royalties. The other authors declare that they have no known competing financial interests or personal relationships that could have appeared to influence the work reported in this paper.

Acknowledgments

This article is considered a product in the framework of the project "Formulation of an integral strategy to reduce the impact on public and environmental health due to the presence of asbestos in the territory of the Department of Bolivar", financed by the General System of Royalties of Colombia (SGR) and identified with the code BPIN 2020000100366. This project was executed by the University of Cartagena, Colombia, and the Asbestos-Free Colombia Foundation. Finally, the authors thank Federico Frassy for his support on the hyperspectral data management and classification, Aiken Hernando Ortega Heredia, María Angélica Narvaez Cuadro, Carlos Andrés Castrillón Ortiz, Michelle Cecilia Montero Acosta, Margareth Peña Castro, Carlos David Arroyo Angulo and the rest of the research group team for logistical support and sample collection in the field. Finally, the authors thank Juan Manuel Gonzales of BlackSquare company for the support in the hyperspectral data acquisition and Sean Fitzgerald for PLM analysis.

Annex 1

Table A1
PLM Sample result

Sample Number	Chrysotile (%vol)	Crocidolite (%vol)	Amosite (%vol)	Cellulose (%vol)
1	–	–	–	28
2	30	–	–	2
3	33	–	–	3
4	35	5	–	–
5	38	6	–	–
6	–	–	–	30
7	–	–	–	35
8	–	–	–	30
9	–	–	–	8
10	40	10	–	–
11	35	10	–	–
12	33	8	–	–
13	40	–	–	–
14	50	–	–	–
15	50	–	–	–
16	–	–	–	35
17	40	8	–	–
18	45	–	–	–
19	42	–	–	6
20	40	15	–	–
21	38	–	–	12
22	–	–	–	40
23	37	8	–	–
24	30	–	–	–
25	32	12	–	–
26	40	10	–	–
27	–	–	–	40
28	38	–	–	5

(*continued on next page*)

Table A1 (*continued*)

Sample Number	Chrysotile (%vol)	Crocidolite (%vol)	Amosite (%vol)	Cellulose (%vol)
29	42	–	–	2
30	47	–	–	–
31	50	–	–	–
32	55	–	–	–
33	44	–	–	–
34	55	–	–	–
35	45	12	–	–
36	45	–	–	–
37	38	–	–	–
38	40	–	–	7
39	44	–	–	–
40	40	–	–	–
41	50	–	–	–
42	48	–	–	8
43	46	–	–	–
44	38	15	–	–
45	45	–	–	9
46	47	–	–	7
47	30	20	–	–
48	27	9	–	–
49	35	–	–	–
50	50	–	–	–
51	48	–	–	–
52	48	–	–	5
53	50	–	–	5
54	47	–	–	–
55	33	–	–	7
56	38	–	–	8
57	40	–	–	10
58	50	5	–	–
59	42	11	–	–
60	40	–	–	8
61	–	–	–	28
62	32	–	–	8
63	48	–	–	–
64	50	–	–	–
65	40	–	–	12
66	38	8	–	–
67	45	–	–	7
68	–	–	–	30
69	40	10	–	–
70	45	11	–	–
71	38	–	–	–
72	40	–	–	5
73	38	–	–	–
74	40	–	–	12
75	45	–	–	9
76	42	–	–	8
77	–	–	–	30
78	45	–	–	–
79	50	–	–	10
80	40	18	–	–
81	50	–	–	–
82	38	–	–	–
83	52	–	–	–
84	–	–	–	28
85	38	8	–	–
86	40	–	–	–
87	37	11	–	–
88	40	10	–	–
89	50	–	–	–
90	55	–	–	–
91	50	–	–	–
92	50	–	–	–
93	55	–	–	–
94	53	–	–	–
95	38	10	–	–
96	37	18	–	–
97	50	–	–	–
98	–	–	–	28

(*continued on next page*)

Table A1 (*continued*)

Sample Number	Chrysotile (%vol)	Crocidolite (%vol)	Amosite (%vol)	Cellulose (%vol)
99	37	–	–	2
100	40	–	–	–
101	32	6	–	4
102	40	40	–	–
103	35	10	–	–
104	45	10	–	–
105	45	10	–	–
106	20	–	–	8
107	43	10	–	3
108	32	8	–	Trace
109	33	–	–	–
110	28	–	–	–
111	28	–	–	–
112	27	–	–	5
113	27	–	–	2
114	30	15	–	1
115	37	–	–	3
116	28	–	–	6
117	30	–	–	7
118	–	–	–	32
119	27	16	–	–
120	27	–	–	15
121	–	–	–	35
122	27	–	–	Trace
123	36	–	–	Trace
124	27	–	–	–
125	32	–	6	–
126	33	–	–	2
127	20	–	–	25
128	32	–	–	–
129	37	–	–	12
130	35	–	–	4
131	38	–	–	–
132	35	–	–	–
133	28	4	–	3
134	30	–	–	–
135	–	–	–	35
136	–	–	–	–
137	30	10	–	–
138	33	–	–	–
139	26	–	–	–
140	35	5	–	2
141	35	2	–	–
142	27	–	–	5
143	26	2	–	7
144	26	–	–	–
145	–	–	–	35
146	30	–	–	4
147	30	–	–	2
148	28	–	–	4
149	35	–	–	Trace
150	30	2	–	–
151	28	–	–	7
152	29	8	–	–
153	38	–	–	–
154	–	–	–	–
155	27	–	–	9
156	36	–	–	5
157	35	–	–	4
158	32	–	–	7
159	36	–	–	–
160	28	–	–	1
161	20	8	–	10
162	37	4	–	–
163	27	–	–	8
164	40	–	–	9
165	39	12	–	–
166	33	–	–	–
167	35	–	–	–
168	33	22	–	–

(*continued on next page*)

Table A1 (*continued*)

Sample Number	Chrysotile (%vol)	Crocidolite (%vol)	Amosite (%vol)	Cellulose (%vol)
169	40	–	–	–
170	–	–	–	29
171	52	–	–	–
172	42	–	–	–
173	22	8	–	–
174	20	–	–	–
175	47	–	–	–
176	50	–	–	–
177	48	–	–	–
178	–	–	–	30
179	–	–	–	28
180	–	–	–	31
181	–	–	–	33
182	45	–	–	–
183	49	–	–	–
184	50	–	–	–
185	–	–	–	35
186	38	–	–	–
187	–	–	–	22
188	37	–	–	–
189	35	–	–	–
190	36	–	–	–
191	30	8	–	–
192	27	–	–	5
193	35	–	–	9
194	–	–	–	30
195	46	–	–	4
196	50	–	–	5
197	39	13	–	–
198	42	15	–	–
199	46	–	–	3
200	50	–	–	–
201	40	–	–	–
202	36	–	–	–
203	35	15	–	–
204	45	–	–	–
205	42	17	–	–
206	43	–	–	2
207	38	–	–	4
208	40	–	–	–
209	50	–	–	–
210	48	–	–	–
211	45	15	–	–
212	47	–	–	–
213	45	–	–	3
214	43	–	–	–
215	51	–	–	4

References

[1] WHO, Asbestos, Geneva, Switzerland, 2020, https://www.who.int/ipcs/assessment/public_health/asbestos/en/.

[2] J.M. Ramada Rodilla, B. Calvo Cerrada, C. Serra Pujadas, G.L. Delclos, F.G. Benavides, Fiber burden and asbestos-related diseases: an umbrella review, Gac. Sanit. 36 (2022) 173–183, https://doi.org/10.1016/j.gaceta.2021.04.001.

[3] A. Moteallemi, M. Minaei, M. Tahmasbizadeh, S. Fadaei, K. Masroor, F. Fanaei, Monitoring of Airborne Asbestos Fibers in an Urban Ambient Air of Mashhad City, Iran: Levels, Spatial Distribution and Seasonal Variations, 2020, https://doi.org/10.1007/s40201-020-00541-5/.

[4] M.B. Stuart, A.J.S. McGonigle, J.R. Willmott, Hyperspectral imaging in environmental monitoring: a review of recent developments and technological advances in compact field deployable Systems, Sensors 19 (2019), https://doi.org/10.3390/S19143071, 3071.

[5] M.J. Khan, H.S. Khan, A. Yousaf, K. Khurshid, A. Abbas, Modern trends in hyperspectral image analysis: a review, IEEE Access 6 (2018) 14118–14129, https://doi.org/10.1109/ACCESS.2018.2812999.

[6] L.K. Torres Gil, D. Valdelamar Martínez, M. Saba, The widespread use of remote sensing in asbestos, vegetation, oil and gas, and geology applications, Atmosphere 14 (2023) 172, https://doi.org/10.3390/atmos14010172.

[7] F. Frassy, G. Candiani, M. Rusmini, P. Maianti, A. Marchesi, F.R. Nodari, G.D. Via, C. Albonico, M. Gianinetto, Mapping asbestos-cement roofing with hyperspectral remote sensing over a large mountain region of the Italian western alps, Sensors 14 (2014) 15900–15913, https://doi.org/10.3390/s140915900.

[8] L. Carlos Chicaíza-Rojas, J. Francisco Lopez-Parra, Uso de imágenes satelitales para detección y cuantificación de asbesto, DYNA 81 (2014) 1–2. https://repository.javeriana.edu.co/bitstream/handle/10554/52636/Anexo.

[9] M.B.A. Gibril, H.Z.M. Shafri, A. Hamedianfar, New semi-automated mapping of asbestos cement roofs using rule-based object-based image analysis and Taguchi optimization technique from WorldView-2 images, Int. J. Remote Sens. 38 (2017) 467–491, https://doi.org/10.1080/01431161.2016.1266109.

[10] C. Bassani, R.M. Cavalli, F. Cavalcante, V. Cuomo, A. Palombo, S. Pascucci, S. Pignatti, Deterioration status of asbestos-cement roofing sheets assessed by analyzing hyperspectral data, Remote Sens. Environ. 109 (2007) 361–378, https://doi.org/10.1016/j.rse.2007.01.014.

[11] M. Norman, H.Z. Mohd Shafri, M.O. Idrees, S. Mansor, B. Yusuf, Spatio-statistical Optimization of Image Segmentation Process for Building Footprint Extraction Using Very High-Resolution WorldView 3 Satellite Data, 2019, pp. 1124–1147, https://doi.org/10.1080/10106049.2019.1573853.

[12] D. Abriha, Z. Kovács, S. Ninsawat, L. Bertalan, B. Balázs, S. Szabó, Identification of roofing materials with discriminant function analysis and random forest classifiers on pan-sharpened WorldView-2 imagery – a comparison, Hungarian Geogr. Bull. 67 (2018) 375–392, https://doi.org/10.15201/HUNGEOBULL.67.4.6.

[13] M. Krówczyńska, E. Raczko, N. Staniszewska, E. Wilk, Asbestos-cement roofing identification using remote sensing and convolutional neural networks (CNNs), Remote Sens. 12 (2020) 1–16, https://doi.org/10.3390/rs12030408.

[14] C. Cilia, C. Panigada, M. Rossini, G. Candiani, M. Pepe, R. Colombo, Mapping of asbestos cement roofs and their weathering status using hyperspectral aerial images, ISPRS Int. J. Geo-Inf. 4 (2015) 928–941, https://doi.org/10.3390/ijgi4020928.

[15] G. Bonifazi, G. Capobianco, S. Serranti, Asbestos containing materials detection and classification by the use of hyperspectral imaging, J. Hazard. Mater. 344 (2018) 981–993, https://doi.org/10.1016/j.jhazmat.2017.11.056.

[16] E. Raczko, M. Krówczyńska, E. Wilk, Asbestos roofing recognition by use of convolutional neural networks and high-resolution aerial imagery. Testing different scenarios, Build. Environ. 217 (2022), https://doi.org/10.1016/j.buildenv.2022.109092.

[17] G. Bonifazi, G. Capobianco, R. Gasbarrone, S. Serranti, S. Bellagamba, D. Taddei, Data fusion of PRISMA satellite imagery for asbestos-containing materials. An application on Balangero's mine site (Italy), Improvement 2022 (2022) 150–157, https://doi.org/10.5220/0011059400003209.

[18] M. Peña-Castro, M. Montero-Acosta, M. Saba, A critical review of asbestos concentrations in water and air, according to exposure sources, Heliyon 9 (2023) e15730, https://doi.org/10.1016/J.HELIYON.2023.E15730.

[19] Law 1968 of July 11, Congress of the Republic of Colombia, 2019, https://www.minambiente.gov.co/documento-normativa/ley-1968-de-2019/. Bogota D.C., Colombia.

[20] UNESCO, Port, Fortresses and group of monuments, Cartagena, Colombia, 1, https://whc.unesco.org/archive/repcom84.htm, 1984.

[21] D. Throsby, Investment in urban heritage conservation in developing countries: concepts, methods and data, City, Cult. Soc. 7 (2016) 81–86, https://doi.org/10.1016/j.ccs.2015.11.002.

[22] HySpex, HySpex Mjolnir VS-620 - Datasheet, HySpex, 2022, p. 1. https://www.hyspex.com/hyspex-products/hyspex-mjolnir/hyspex-mjolnir-vs-620/.

[23] G. Lixin, X. Weixin, P. Jihong, Segmented minimum noise fraction transformation for efficient feature extraction of hyperspectral images, Pattern Recognit. 48 (2015) 3216–3226, https://doi.org/10.1016/j.patcog.2015.04.013.

[24] F. Frassy, G. Dalla Via, P. Maianti, A. Marchesi, F.R. Nodari, M. Gianinetto, Minimum noise fraction transform for improving the classification of airborne hyperspectral data: two case studies, Work. Hyperspectral Image Signal Process, Evol. Remote Sens. (2013), https://doi.org/10.1109/WHISPERS.2013.8080626, 2013-June.

[25] G. Luo, G. Chen, L. Tian, K. Qin, S.-E. Qian, Minimum noise fraction versus principal component analysis as a preprocessing step for hyperspectral imagery denoising, Can. J. Remote Sens. 42 (2016) 106–116, https://doi.org/10.1080/07038992.2016.1160772.

[26] A.A. Green, M. Berman, P. Switzer, M.D. Craig, A transformation for ordering multispectral data in terms of image quality with implications for noise removal, IEEE Trans. Geosci. Remote Sens. 26 (1988) 65–74, https://doi.org/10.1109/36.3001.

[27] D. Ballabio, R. Todeschini, Multivariate classification for qualitative analysis, in: Infrared Spectrosc. Food Qual. Anal. Control, Academic Press, 2009, pp. 83–104, https://doi.org/10.1016/B978-0-12-374136-3.00004-3.

[28] A.F. Oberta, L. Poye, S.P. Compton, Releasability of asbestos fibers from weathered roof cement, J. Occup. Environ. Hyg. 15 (2018) 466–473, https://doi.org/10.1080/15459624.2018.1448401.

[29] US EPA, Conference on encapsulation of asbestos-containing building materials: transcript of proceedings, vol. 1, in: Acme Reporting Company, Arlington, Virginia, 1981, pp. 1–198.

[30] S. Bolan, L. Kempton, T. McCarthy, H. Wijesekara, U. Piyathilake, T. Jasemizad, L.P. Padhye, T. Zhang, J. Rinklebe, H. Wang, M.B. Kirkham, K.H.M. Siddique, N. Bolan, Sustainable management of hazardous asbestos-containing materials: containment, stabilization and inertization, Sci. Total Environ. 881 (2023) 163456, https://doi.org/10.1016/j.scitotenv.2023.163456.

[31] A. Obmiński, J. Janeczek, The effectiveness of asbestos stabilizers during abrasion of asbestos-cement sheets, Constr. Build. Mater. 249 (2020) 118767, https://doi.org/10.1016/J.CONBUILDMAT.2020.118767.

[32] J.R. Navarro-Vargas, G.A. Villamizar, Asbestos ban. What comes after the adoption of Act 1968 of 2019? Rev. La Fac. Med. 67 (2019) 1. https://www.redalyc.org/journal/5763/576366818001/movil/.

[33] G. Villamizar, G. Camero, Asbesto en Colombia. Fundamentos para el debate, Bogotá, 2019.

[34] FUNDCLAS, Manejo del Asbesto: Guía de buenas prácticas para reducir el riesgo de exposición al asbesto instalado, Asbestos s, Bogotá, Colombia, 2021. https://drive.google.com/drive/folders/1cXwju91aPsDEhEz7CC_FbxRnU11vRg2s.

[35] Toscana Region, Plan for Environmental Protection, Decontamination, Disposal and Remediation for the Purpose of Defense against the Dangers Deriving from Asbestos, Florence, Italy, 1997. http://www.assoamianto.it/deliberazione_consiglio_regionale.htm.

[36] Emilia Romagna Region, Guidelines for Assessing the State of Conservation of Cement-Asbestos Roofing and for Risk Assessment, Bologna, Italy, 2021.

[37] K. Spurny, H. Marfels, C. Boose, G. Weiss, H. Opiela, F.J. Wulbeck, Fiber emissions from weathered asbestos cement products. 2. Physical-chemical properties of liberated asbestos fibers, Zentralbl. Hyg. Umweltmed. 188 (1989) 262–270. https://pubmed.ncbi.nlm.nih.gov/2547393/.

[38] J.R. Thomas, H.W. Gausman, Leaf reflectance vs. Leaf chlorophyll and carotenoid concentrations for eight crops, Agron. J. 69 (1977) 799–802, https://doi.org/10.2134/agronj1977.00021962006900050017x.

[39] E. Raymond Hunt, C.S.T. Daughtry, J.U.H. Eitel, D.S. Long, Remote sensing leaf chlorophyll content using a visible band index, Agron. J. 103 (2011) 1090–1099, https://doi.org/10.2134/AGRONJ2010.0395.

[40] J. Dash, P.J. Curran, The MERIS terrestrial chlorophyll index, 2010, https://doi.org/10.1080/0143116042000274015, 5403–5413.

[41] R.N. Clark, T.L. Roush, Reflectance spectroscopy: quantitative analysis techniques for remote sensing applications, J. Geophys. Res. 89 (1984) 6329–6340, https://doi.org/10.1029/JB089iB07p06329.

[42] S. Kotthaus, Spectral Library of Impervious Urban Materials, London, UK, 2013, http://www.met.reading.ac.uk/micromet/documents/LUMA_SLUM.pdf.

[43] R.F. Kokaly, R.N. Clark, G.A. Swayze, K.E. Livo, T.M. Hoefen, N.C. Pearson, R.A. Wise, W.M. Benzel, H.A. Lowers, R.L. Driscoll, A.J. Klein, USGS spectral library version 7: U.S, Geol. Surv. Data Ser. 1035 (2017), https://doi.org/10.3133/ds1035.

[44] P. Tadas, M. Dainius, K. Edvinas, K. Linas, K. Maksim, Z. Axel, Comparative characterization of particle emissions from asbestos and non-asbestos cement roof slates, Build. Environ. 46 (2011) 2295–2302, https://doi.org/10.1016/j.buildenv.2011.05.010.

[45] S.-H. Park, Types and health hazards of fibrous materials used as asbestos substitutes, Saf. Health Work. 9 (2018) 360–364, https://doi.org/10.1016/j.shaw.2018.05.001.

[46] I. Elfaleh, F. Abbassi, M. Habibi, F. Ahmad, M. Guedri, M. Nasri, C. Garnier, A comprehensive review of natural fibers and their composites: an eco-friendly alternative to conventional materials, Results Eng. 19 (2023) 101271, https://doi.org/10.1016/j.rineng.2023.101271.

[47] S. Szabó, P. Burai, Z. Kovács, G. Szabó, A. Kerényi, I. Fazekas, M. Paládi, T. Buday, G. Szabó, Testing algorithms for the identification of asbestos roofing based on hyperspectral data, Environ. Eng. Manag. J. 143 (2014) 512900, https://doi.org/10.30638/eemj.2014.323.

[48] L. Fiumi, A. Campopiano, S. Casciardi, D. Ramires, Method validation for the identification of asbestos–cement roofing, Appl. Geomatics 4 (2012) 55–64, https://doi.org/10.1007/s12518-012-0078-0.

[49] M. Norman, H.Z.M. Shafri, S.B. Mansor, B. Yusuf, Review of remote sensing and geospatial technologies in estimating rooftop rainwater harvesting (RRWH) quality, Int. Soil Water Conserv. Res. 7 (2019) 266–274, https://doi.org/10.1016/j.iswcr.2019.05.002.

[50] Y. Suzuki, S.R. Yuen, R. Ashley, Short, thin asbestos fibers contribute to the development of human malignant mesothelioma: pathological evidence, Int. J. Hyg. Environ. Health 208 (2005) 201–210, https://doi.org/10.1016/j.ijheh.2005.01.015.
[51] S. Serranti, G. Bonifazi, 20 - detection and classification of asbestos and other contaminants in C&DW by advanced technologies, in: F. Pacheco-Torgal, Y. Ding, F. Colangelo, R. Tuladhar, A. Koutamanis (Eds.), Adv. Constr. Demolition Waste Recycl., Woodhead Publishing, 2020, pp. 407–437, https://doi.org/10.1016/B978-0-12-819055-5.00020-6.
[52] National Geographic, Deserts, Explained, 1, https://www.nationalgeographic.com/environment/article/deserts, 2023 (accessed September 22, 2023).